Temperature-Energy Relationships and Spatial Distribution Analysis for Nano-Enhanced Phase Change Materials Via Thermal Energy Storage

Florence Awuor Misawo[1]; Fredrick O. Nyamwala[2]
Department of Mathematics School of Biological & Physical
Science Moi University, Eldoret Kenya

Thomas T. O. Onyango[3]
Department of Pure and Applied Mathematics,
Technical University of Kenya

Abstract:- Despite the abundance and affordability of solar energy, its adoption in industrial and domestic sectors, especially in developing countries, still needs to be improved. This study addresses the gap by proposing integrated storage systems to align energy supply and demand, essential for various industrial processes. Investigating Nano-enhanced Phase Change Material (PCM), the research formulates governing equations for the phase change process, explores numerical simulations using MATLAB's Finite Volume Method, and validates models. The PCM comprises a solid salt mixture with Sodium Chloride Nanoparticles. The analysis of nano-enhanced PCMs for thermal energy storage focuses on understanding the interrelationship between temperature, energy, and nanoparticle distribution within the PCM. Visuals based on 3D surface plots and scatter plots illustrate how energy storage characteristics vary with temperature and spatial variables, identifying phase change temperatures and energy absorption/release points. These visualizations guide PCM optimization for improved thermal conductivity and heat capacity, which is crucial for diverse applications like solar energy systems and thermal management in electronics. Nano-enhanced PCM performance can be further enhanced by employing advanced numerical methods and simulation tools for accurate prediction and optimization before experimental validation.

Keywords:- *Nano-Enhanced Phase Change Materials; Phase Change Process; Energy Storage; Finite Volume Method.*

I. INTRODUCTION

A. Background Information

The quest for clean, sustainable sources of energy is becoming more popular with the concerns over global warming [32]. Scientists have established that carbon dioxide emissions, from the use of fossil fuels contribute to the greenhouse effect. Solar energy is unlimited and harnessing it for heating and electricity is pollution free. Development of solar energy equipment among them being solar cookers can help our environment by decreasing emissions [17]. In addition, solar energy is renewable and readily available. One major drawback in harnessing is its availability only during sunshine, presenting major challenge to its use in the dark. Solar radiation is intermittent, irregular in nature and its storage is essential in order to optimize its usage.

Collection of solar energy is done by the use of a parabolic trough as shown in Figure 1. This is then directed to a focal point where the receiver stands to absorb it. Vapor is generated in the heat absorber at the focal point of the parabolic concentrator and condensed in a coiled tube, which is casted into an aluminum plate [22]. Heat transfer is by a thermo-syphon principle, with water as the working fluid at about 35-bar pressure. The heating plate has heat-conducting rods extended into a phase change storage system (Nitrate mixture). Thermal energy is stored in the form of Latent heat which the research is based via Partial Differential Equations (PDEs).
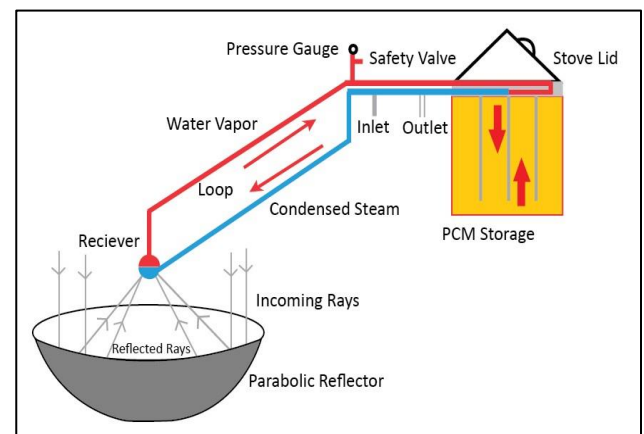

Fig 1: Illustration on Collection and Storage of Solar Energy

The basic mechanisms of heat transfer are conduction, convection and radiation [36]. Conduction is the transfer of energy from the more energetic particles of a substance to the adjacent less energetic ones as a result of interaction between particles. Convection is the mode of heat transfer between a solid surface and adjacent liquid or gas which is in motion and it involves the combined effects of conduction and fluid motion. According to [34], transfer of solar energy by radiation is where the energy emitted by matter is in the form of electromagnetic waves (or photons) as a result of the changes of the electronics configuration of the atoms or molecules.

There are three forms of heat energy storage namely sensible heat, latent heat and thermo-chemical or combination of these [12]. Sensible heat storage (SHS) is a criterion for storing thermal energy by raising the temperature of a solid or liquid [6]. SHS system utilizes heat capacity and change in temperature of the material during the process of charging and discharging. The amount of heat stored depends on the specific heat of the medium, the temperature change and the amount of storage material.

Total enthalpy H is computed as the sum of the sensible enthalpy, h and the latent heat $\triangle H$ [44]

$$H = h + \triangle H \tag{1}$$

Where

$$h = h_{ref} + \int_{T_{ref}}^{T} C_p dT \tag{2}$$

In quation (2) h_{ref} and T_{ref} denote the reference enthalpy and reference temperature respectively, C_p represents the specific heat. $\triangle H = f_1 L$, where L is the latent heat of PCM and f_1 is the liquid fraction.

Latent heat storage (LHS) is based on the heat absorption or release when a storage material undergoes a phase change from solid to liquid or liquid to gas or vice versa at constant temperature [25]. Latent heat is an attractive way to store solar thermal energy as it provides high storage density where a lot of energy can be stored in a very small volume. The phase change process occurs at nearly constant temperature, which is a fundamental aspect for efficient operation of most thermal systems [31]. An advantage of LHS relative to SHS is that the temperature of the phase change material (PCM) may be closer to the environment temperature thereby minimizing heat loss or gain. In addition, the driving temperature of a LHS system can remain nearly constant between a heat transfer surface and the PCM during both charging and discharging which may vary greatly during operation for the SHS system. These properties along with the higher energy density make LHS an attractive form of thermal storage, particularly for portable appliances which is not practical for SHS systems [35].

The principle of thermochemical heat storage uses the energy from an exothermic reaction for the application, and charge the storage by running the corresponding endothermic reaction [18]. The storage potential of thermochemical energy is very important and research on improvements are intensively conducted both for large size seasonal and small size modules. PCM is a substance having a high heat of fusion which, on melting and solidifying at a certain temperature is capable of storing and releasing large amounts of energy. Solid liquid PCMs have a unique advantage of negligible volume expansion between solid crystalline structures along with the elimination of leaks [28].

Alot of studies have been performed on PCMs for the last three decades which are found to be very interesting due to their ability to store large amount of energy as latent heat at a constant phase transition temperature [46, 5, 39, 40]. However, some of disadvantages such as low thermal conductivity which impedes high rate of charge and discharge of heat flux were observed. The PCMs have many useful properties including heat source at constant temperature, heat recovery with small temperature drop, high storage density, melting point which matches the applications, low vapor pressure (1 bar) at the operational temperature, and chemical stability and non-corrosiveness.

The choice of PCM is based on the melting temperature, the latent heat of fusion, density and other considerations such as toxicity, corrosiveness and cost [15]. As one of the goals of latent energy storage is to achieve a high storage density in a relatively small volume, PCMs should have a high melting enthalpy kJ/Kg and a high density (Kg/m^2), that is, a high volumetric melting enthalpy [16]. No single material can have all the required properties for an ideal thermal storage media [30]. Practical difficulties include; low thermal conductivity, density change, stability of properties under extended cycling, phase segregation and sub-cooling of PCM. Among the materials for phase change are Sodium Nitrate (melting point 308^0C, density $2.26g/cm^3$, specific heat $93.05j/(molK)$ and Potassium Nitrate (melting point 334^0C, density $2.11g/cm^3$, specific heat $95.06j/(molK)$.

In order to increase thermal conductivity of a PCM, several heat transfer enhancement techniques have been studied such as incorporating high thermal conductivity enhancers such as nanoparticles into PCM and porous heat transfer media, extending heat transfer surfaces by fins and capsules, using intermediate heat transfer medium or heat pipes and employing multiple PCMs [31]. Heat transfer improves when thermal penetration depth or heat diffusion is increased. Other common enhancement techniques include addition of high thermal conductivity materials such as nanoparticles, extended surfaces, structures and heat pipes, as well as utilizing encapsulation and cascaded configurations. Combination of two or more of the aforementioned techniques, enhances heat transfer rates considerably [21].

B. Contribution

The low thermal conductivity of PCMs impedes the high rate of charge and discharge of heat flux. Heat transfer enhancement techniques, such as incorporating nano-particles into PCMs, using porous heat transfer media, and employing multiple PCMs improve thermal conductivity. The choice of PCM is critical, considering factors like melting temperature, latent heat of fusion, density, toxicity, corrosiveness, and cost. The criteria for selecting PCMs, need to emphasize on the need for high volumetric melting enthalpy. This is because no single material may possess all the required properties for an ideal thermal storage medium. Practical difficulties in PCM applications such as low thermal conductivity, density change, stability under extended cycling, phase segregation, and sub-cooling. This

can be addressed by achieving an ideal thermal storage medium. Thus addressing these practical difficulties is crucial for the successful implementation of PCM-based energy storage systems.

II. RELATED WORKS

The finite volume method (FVM), sometimes referred to as the control volume method, was introduced by [2], developed for solving heat transfer and fluid flow problems. FVM is a discretization technique for partial differential equations, especially those that arise from physical conservation laws and are discretized or transformed into a set of algebraic equations a computer can solve.

The main advantage of FVM over others like the FDM and FEM is its close connection to the underlying factors of conservation of laws (conservation of mass, conservation of energy, conservation of momentum) [37]. FVM ensures that quantities remain conserved at discrete levels; this agrees with the law of physics at all discretisation levels. It divides the domain into a finite number of non-overlapping cells or control volumes over which conservation (piecewise linear profile between any two points) is enforced in a discrete sense.

FVM can also be applied to various mesh structures and geometries [20]. It is applied in both unstructured and structured mesh quite well. Within each node in the mesh, a control volume is constructed over which the governing equations are solved discretely. The two components of discretization in FVM are the approximation of the flux through a control volume face by numerical integration over the face and the evaluation of the functions and gradients.

PCM-based thermal storage devices offer a versatile, sensible, and latent heat storage solution. They are precious in applications where temperature control, high energy density, and reduced heat loss are essential. Ongoing research and development in PCM technology will likely lead to improved materials and broader adoption in various sectors, including renewable energy, buildings, and industrial processes. For instance, [27] explores three critical parameters: fin arrangement, fin shape, and the number of fins in PCM. Among these parameters, the configuration with eight fins, where the bottom fin length increases while compensating for reduced side fin length, is the most effective. This configuration results in an impressive 60.77% reduction in the combined melting and solidification duration, showcasing its potential for enhancing the efficiency of thermal energy storage systems.

[43] introduced a hybrid sensible-latent thermal energy storage (TES) system to overcome issues with single-tank thermocline TES systems, such as quick thermocline degradation and temperature fluctuations during discharge. The study experimentally assesses the system via a combination of sensible heat concrete with axial holes and multiple layers of PCMs. Four configurations were tested: MLSPCM, SLSPCM-1, SLSPCM-2, and SSCB. Results indicated that MLSPCM performance was the best, with an 87% effective discharge efficiency and a storage capacity of 12.53 kWh. Using multilayers of PCM with suitable melting and solidification temperatures and cost-effective sensible concrete, this approach proved to be a viable and economical TES solution for medium-temperature applications.

[1] explored the potential of a cost-effective TES solution for medium-temperature industrial applications like chemical processing and beverages. Traditional single-tank thermocline TES systems face performance issues due to thermocline degradation during discharging. This is solved by the introduction of a novel combined sensible-latent heat configuration. It involved using structured, cost-effective, sensible heat materials with encapsulated phase change material (PCM) capsules, creating cascaded, layered, packed beds within the tank. Numerical simulations evaluated the performance of different configurations, and the results suggested that the TES system with a volume fraction arrangement of (40%-20%-40%) performance was the best, followed by (25%-50%-25%) and (10%-80%-10%), respectively. The single-layered sensible rod with PCM (SLSPCM) arrangement performance was the least effective. This approach, which involved multistage PCMs with suitable characteristics and cost-effective structured filler material, offered an efficient and economical TES alternative.

[41] explored the cascade latent heat thermal energy storage (LHTES) system by combining one unit of erythritol and two units of paraffin wax with a melting point of approximately 60^0C, effectively recovering medium-temperature industrial waste heat (150–180°C). This system addresses the limitations of single-PCM by absorbing waste heat below erythritol's melting point (around 118 °C) during charging and supplying heat above paraffin wax's melting point during discharging. Prototype testing confirmed its superior performance, increasing waste heat recovery efficiency from 15.8% to 63.4% at 100 L/h and 160°C compared to a single-stage erythritol-based system. An active discharging strategy also raised the average heat supply temperature from 37 °C (with a constant flow rate) to 53.6 °C. This highly efficient cascade LHTES system promises to decarbonize building space heating by recovering medium-temperature waste heat.

III. PROPOSED METHOD

The numerical scheme simulates the solid-liquid phase change process using mathematical models described by conservation and solving PDE [45]. Mathematical models were derived by considering a smooth interface enthalpy method on a fixed grid and structured mesh and formulating governing equations for PCM with and without nanoparticles. FVM did discretization of the domain and governing equations. This was achieved by applying the divergence theorem to convert volume integrals to surface integrals for each control volume. Function values and flux were approximated from the centre of control volumes. The PDEs obtained were thus transformed into a set of algebraic equations to be solved by MATLAB. These specify the contributions of the Nanoparticles in the heat storage system.

In physical geometry, solar energy is the source of thermal energy conveyed by hot water, transported by gravity, then stored in the PCM during the melting process as latent heat and released at an appropriate time during the solidification process. A small desirable amount of Sodium Chloride volume fractions acting as Nanoparticles is added to the PCM. A solid salt mixture of Sodium Nitrate and Potassium Nitrate mixed in the ratio of $3:2$. Heat transfer is more enhanced in large surface areas; thus, spherical shapes with a diameter of 100 nm nanoparticles are preferred for the study.

A. Models for Phase Change Process

The mathematical models are derived by assuming a smooth interface with thermal conductivity and latent heat of fusion being continuous and differentiable functions of temperature. Mathematical modelling of the phase change process is complex due to the existence of a transition region [11]. A mixture of solid and liquid phases, in which the phase change occurs, results in complex changes in transport properties such as density, specific heat, conductivity, and the latent heat of fusion, which depends on temperature. The phase transition region propagates in spatial directions (its location changes as time elapses), resulting in initial value problems containing singularities at the interfaces and challenging the numerical simulation.

➤ *Sharp-Interface Models*

Sharp-interface models where liquid and solid phases are assumed to be separated by infinitely thin sharp interface [14]. The transport properties such as density, specific heat and conductivity are assumed to experience a jump at the interface. The latent heat of fusion is assumed to be instantaneously released or absorbed at the interface, resulting in step (sharp) change in the transport properties, and mathematical models for liquid and solid phases are derived individually. Disadvantages of this model are that a sharp interface leads to a mathematical model in which the initial value problem contains singularity at the interface and that spatial location during evolution requires front-tracking methods.

➤ *Phase Field Models*

Phase field models where the solid and liquid phases are also assumed to be separated by a finite width (in temperature) transition region, where transport properties are assumed to vary with temperature between the two states [23]. The method is based on the specification of free energy density functional, which is the main driving force for the movement of the phase transition region. The models eliminate the sharp interfaces and their tracking, but alongside these, there are some disadvantages. A priori knowledge of the free energy density functional for the application at hand is required; the mathematical model cannot simulate the initiation or formation of the solid-liquid interface; hence, the liquid-solid phases and the transition region must be defined as initial conditions. This limitation is due to the specific nature of the free energy function. However, if a liquid-solid interface is specified as an initial condition, then the phase field models are quite effective in simulating the movement of the front during evolution. In most applications of interest, simulation of initiation of the transition region is important as it may not be possible to know its location and the precise conditions under which it initiates a priori. These limitations have resulted in minimal widespread use of these mathematical models in practical applications.

➤ *Enthalpy Approach*

The enthalpy approach is where the energy equation is recast in terms of enthalpy and temperature, keeping them as dependent variables in the mathematical model [42]. Computations of numerical solutions of the resulting initial value problem are performed on a fixed discretization. This approach eliminates the energy balance equation at the interface used in the sharp interface models and introduces a finite phase transition region (over a small temperature change) called a mushy region between the liquid and the solid phases. The transport properties are assumed to vary in some manner from one phase to the other phase. The concept of liquid or solid fraction is generally introduced to account for the mushy region being a mixture of solid and liquid phases [38]. Due to the assumption of the mushy region separating the solid and the liquid phases, the sharp interface and the associated problems, such as singularity, are inhibited, giving the approach an advantage over the others in numerical computations of the evolution of phase change problems. The Darcy law for porous media is adopted to model the flow of PCM in the mushy region [47]. The law is based on the empirical measurement of permeability and is expressed as

$$u_i = -\frac{K}{\mu}\left\{\frac{\partial P}{\partial x_i} - \rho g_{xi}\right\} \tag{3}$$

Where K is the permeability, in the case of a mushy region of commercial material, a function of liquid fraction; in the model, permeability decreases with decreasing liquid fraction; consequently, it forces all the velocities to become zero in the case of a stationary solid. The coefficient $\frac{K}{\mu}$ decreases from a significant value in the solid phase to zero in the liquid phase. As a result, the Darcy source term vanishes as the liquid fraction becomes 1. The mathematical models derived and presented here are the same as those in Lagrangian and Eulerian descriptions. They are based on the first law of thermodynamics using specific total energy and the heat vector augmented by the constitutive equation for the heat vector.

In this study, mathematical models are derived based on the assumption that the stress field is constant and the velocity field is zero in the solid region but nonzero in the liquid region. In the transition zone, the stress and the velocities are assumed to make the transition from a nonzero state in the fluid to a constant stress state and zero velocity in the solid phase based on the temperature with the assumption that the solid particles in the transition region form a porous medium through which the fluid flows. The enthalpy approach for the phase change is preferred, considering the space-time coupled approximation method.

B. Boundary Conditions

There are three types of boundary conditions (BC) which can be developed and imposed on the coupled governing equations to make them well-posed and solvable, namely, Dirichlet boundary condition [3], Neumann boundary condition [8] and Cauchy boundary condition [7]. In Dirichlet Boundary conditions, the value of the function is specified on the boundary, and dependent variables of the governing equations are prescribed in the domain at different points [3]. In Neumann Boundary conditions, the value of the derivative normal to the boundary is specified. A Neumann BC imposed on governing equations specifies the derivative values of a solution to be taken on the boundary of the domain [8]. In Cauchy Boundary conditions, the values involve a linear combination of Dirichlet and Neumann BC to governing equations [7]. A Cauchy BC imposed on governing equations specifies both the values of a solution of a differential equation to take on the domain and the normal derivation at the boundary.

The PCM is enclosed within annular cavity formed between two concentric horizontal cylindrical shells with the inner shell considered to be of a significantly thinned wall subjected to a constant heat flux of 225 ^{0}C (1 ^{0}C higher than the melting point of the PCM) on the southern wall keeping the outer shell (northern wall) at adiabatic condition which simulates the PCM storing thermal energy during charging. The inlet velocity of the melt is 0.003cm/s. The western and eastern walls are also kept at adiabatic condition. The elementary cross-sectional cavity of dimension 10cm (x direction) by 1cm (y direction) is used to model the phase change process as represented by the Fig. 2.
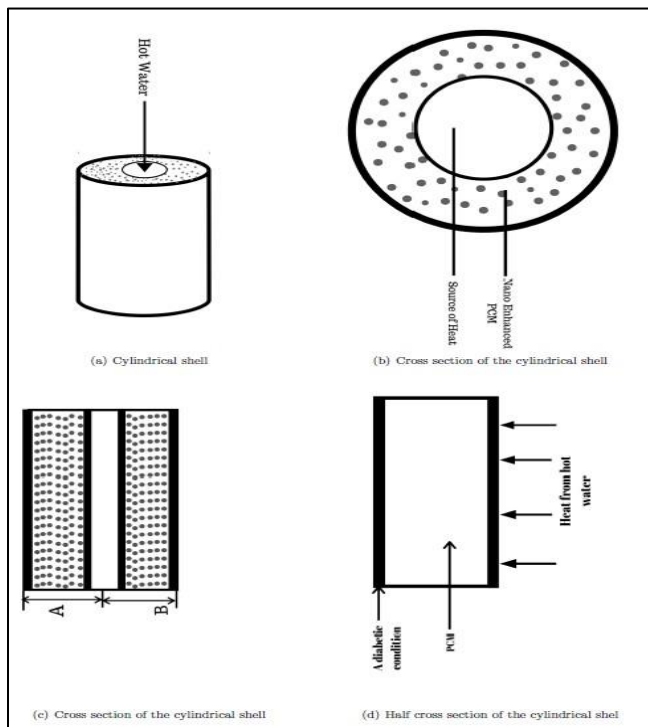

Fig 2: The Elementary Cross-Sectional Cavity of Dimension 10cm (x Direction) by 1cm (y Direction) is used to Model the phase Change Process

C. Discretization of the Partial Differential Equations

FVM is derived based on the integral form of conservation laws. It discretizes the domain into finite control volumes and approximates the total integral of flux over each control volume rather than pointwise approximations at mesh points (see Figure 2). These values are modified on each time step by using the flux through the edges of the grid cells. Discretization of governing equations follows three steps: Space discretization, Time discretization and Equation discretization. Space discretization involves the definition of a numerical grid, which replaces the continuous space with a finite number of discrete elements with computational points at their centroids. At these points, the solution of dependent variables is computed. This process is termed grid generation. Time discretization assumes the division of the entire time interval into a finite number of small sub-intervals, called time steps, which guarantee convergence of the solution. Discretization of equations involves the replacement of the individual terms in the governing equations by algebraic expressions connecting the variable values at computational points in the grid.
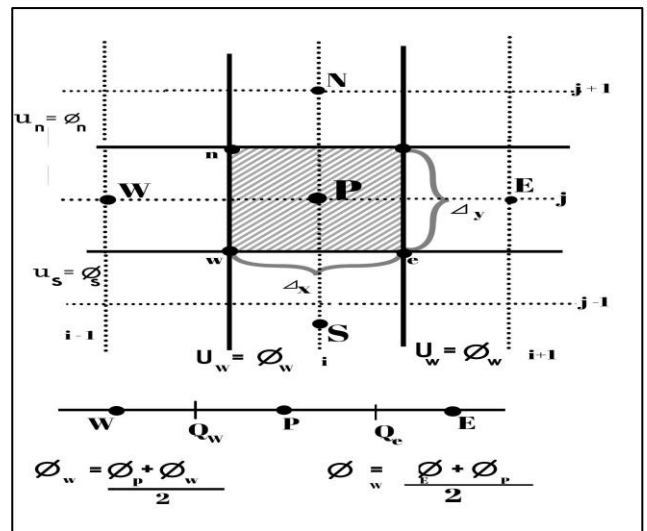

Fig 3: Control Volume

D. Non-dimensionlization and Discretization of the Governing Equations

Non-dimensionlisation is the partial or full removal of physical dimensions from an equation involving physical quantities by a suitable substitution of variables. Reynold's Number being one of the dimensionless number gives a measure of the ratio of inertia(resistant to change or motion) forces to viscous forces. Laminar flows occurs at low Reynolds's Number whereas turbulent flow occurs at high Reynold's number. The following variables are used to non-dimensionalization of the parameters: time, distance, velocity, temperature and pressure as:

$$t^* = \frac{t}{L/U_\infty}, x^* = \frac{x}{L}, y^* = \frac{y}{L}, z^* = \frac{z}{L}, u^* = \frac{u}{U_\infty}, v^* = \frac{v}{U_\infty}, w^* = \frac{w}{U_\infty}, p^* = \frac{p-p_\infty}{\rho/U_\infty^2}, T^* = \frac{T-T_\infty}{\Delta T}.$$

E. Non Dimensionlisation and Discretiastion of Conservation of Mass Equation

The flow of molten PCM is governed by continuity equation and momentum equations expressed in cartesian coordinates. Non dimesionlising, we obtain

$$\nabla = i\frac{\partial}{\partial x} + j\frac{\partial}{\partial y} + k\frac{\partial}{\partial z} \tag{4}$$

$$\vec{V} = ui + vj + wk \tag{5}$$

$$\nabla \cdot \vec{V} = \frac{\partial u}{\partial x} + \frac{\partial v}{\partial y} + \frac{\partial w}{\partial z} \tag{6}$$

In 2-Dimensional, equation 3.8 becomes,

$$\nabla \cdot \vec{V} = \frac{\partial u}{\partial x} + \frac{\partial v}{\partial y} = 0 \tag{7}$$

Non-Dimesionlizing yields

$$\frac{\partial u^* U_\infty}{\partial x^* L} + \frac{\partial v^* U_\infty}{\partial y^* L} = 0 \tag{8}$$

$$\frac{U_\infty}{L}\{\frac{\partial u^*}{\partial x^*} + \frac{\partial v^*}{\partial y^*}\} = 0 \tag{9}$$

$$\frac{\partial u^*}{\partial x^*} + \frac{\partial v^*}{\partial y^*} = 0 \tag{10}$$

Discretisation of conservation of mass equation

$$\int_{y_{(J-\frac{1}{2})}}^{y_{(J+\frac{1}{2})}} \int_{x_{(i-\frac{1}{2})}}^{x_{(i+\frac{1}{2})}} \frac{\partial u^*}{\partial x^*} dxdy + \int_{y_{(J-\frac{1}{2})}}^{y_{(J+\frac{1}{2})}} \int_{x_{(i-\frac{1}{2})}}^{x_{(i+\frac{1}{2})}} \frac{\partial v^*}{\partial y^*} dxdy = 0 \tag{11}$$

$$\int_{y_{(J-\frac{1}{2})}}^{y_{(J+\frac{1}{2})}} \int_{x_{(i-\frac{1}{2})}}^{x_{(i+\frac{1}{2})}} \frac{\partial u^*}{\partial x^*} dxdy + \int_{y_{(J-\frac{1}{2})}}^{y_{(J+\frac{1}{2})}} \int_{x_{(i-\frac{1}{2})}}^{x_{(i+\frac{1}{2})}} \frac{\partial v^*}{\partial y^*} dxdy\} = 0 \tag{12}$$

$$\Delta t \Delta y \int_{x_{(i-\frac{1}{2})}}^{x_{(i+\frac{1}{2})}} \frac{\partial u^*}{\partial x^*} dx + \Delta t \Delta x \int_{y_{(J-\frac{1}{2})}}^{y_{(J+\frac{1}{2})}} \frac{\partial v^*}{\partial y^*} dy = 0 \tag{13}$$

$$\Delta t \Delta y(u^*_{(i+\frac{1}{2})} - u^*_{(i-\frac{1}{2})}) + \Delta t \Delta x(v^*_{(j+\frac{1}{2})} - v^*_{(j-\frac{1}{2})}) = 0 \tag{14}$$

$$\Delta y \Delta t\{(\frac{u^*_{i+1}+u^*_i}{2}) - (\frac{u^*_{i-1}+u^*_i}{2})\} + \Delta x \Delta t\{(\frac{v^*_{j+1}+v^*_j}{2}) - (\frac{v^*_{j-1}+v^*_j}{2})\} = 0 \tag{15}$$

$$\frac{\Delta t \Delta y}{2}(u^*_{i+1} - u^*_{i-1}) + \frac{\Delta x \Delta t}{2}(v^*_{j+1} - v^*_{j-1}) = 0 \tag{16}$$

Simplifying further we obtain,

$$\Delta y(u^*_{i+1} - u^*_{i-1}) + \Delta x(v^*_{j+1} - v^*_{j-1}) = 0 \tag{17}$$

F. Non Dimesionlization of Momentum Equations

Non dimensionlizing equation 5, momentum equation in x-direction using the given variables

$$t^* = \frac{t}{\frac{L}{U_\infty}} \Rightarrow \frac{\partial t^*}{\partial t} = \frac{U_\infty}{L} \text{ and } t = \frac{t^*L}{U_\infty}$$

Substituting with values of u and t in $\frac{\partial u}{\partial t}$, we obtain

$$\frac{\partial u}{\partial t} = \frac{U_\infty^2}{L}\frac{\partial u^*}{\partial t^*} \tag{18}$$

$$x = x^*L \Rightarrow \frac{\partial x^*}{\partial x} = \frac{1}{L}, \quad y = y^*L \Rightarrow \frac{\partial y^*}{\partial y} = \frac{1}{L}, \quad u = u^*U_\infty \Rightarrow \frac{\partial u^*}{\partial x} = 0$$

$$\frac{\partial u}{\partial x} = \frac{\partial(u^*U_\infty)}{\partial x^*}\frac{\partial x^*}{\partial x} = U_\infty \frac{\partial u^*}{\partial x^*}\frac{1}{L} = \frac{U_\infty}{L}\frac{\partial u^*}{\partial x^*} \tag{19}$$

$$\frac{\partial u}{\partial y} = \frac{\partial(u^*U_\infty)}{\partial y^*}\frac{\partial y^*}{\partial y} = U_\infty \frac{\partial u^*}{\partial y^*}\frac{1}{L} = \frac{U_\infty}{L}\frac{\partial u^*}{\partial y^*} \tag{20}$$

We know $\frac{\partial}{\partial x} = \frac{\partial}{\partial x^*}\frac{\partial x^*}{\partial x}, \frac{\partial x^*}{\partial x} = \frac{1}{L}, \frac{\partial u}{\partial x} = \frac{U_\infty}{L}\frac{\partial u^*}{\partial x^*}$ then we obtain,

$$\frac{\partial^2 u}{\partial x^2} = \frac{\partial}{\partial x}\left(\frac{\partial u}{\partial x}\right) = \frac{\partial}{\partial x^*}\frac{\partial x^*}{\partial x}\left(\frac{U_\infty}{L}\frac{\partial u^*}{\partial x^*}\right) = \frac{U_\infty}{L^2}\frac{\partial^2 u^*}{\partial x^{*2}} \tag{21}$$

We also know $\frac{\partial}{\partial y} = \frac{\partial}{\partial y^*}\frac{\partial y^*}{\partial y}, \frac{\partial y^*}{\partial y} = \frac{1}{L}, \frac{\partial u}{\partial y} = \frac{U_\infty}{L}\frac{\partial u^*}{\partial y^*}$ then we obtain,

$$\frac{\partial^2 u}{\partial y^2} = \frac{\partial}{\partial y}\left(\frac{\partial u}{\partial y}\right) = \frac{\partial}{\partial y^*}\frac{\partial y^*}{\partial y}\left(\frac{U_\infty}{L}\frac{\partial u^*}{\partial y^*}\right) = \frac{U_\infty}{L^2}\frac{\partial^2 u^*}{\partial y^{*2}} \tag{22}$$

Substituting equations 23-27 in the momentum equation 5, we obtain,

$$\rho\left(\frac{U_\infty^2}{L}\frac{\partial u^*}{\partial t^*} + u^*U_\infty\frac{U_\infty}{L}\frac{\partial u^*}{\partial x^*} + v^*U_\infty\frac{U_\infty}{L}\frac{\partial u^*}{\partial y^*}\right) = \mu\left(\frac{U_\infty}{L^2}\frac{\partial^2 u^*}{\partial x^{*2}} + \frac{U_\infty}{L^2}\frac{\partial^2 u^*}{\partial y^{*2}}\right) \tag{23}$$

Multiply through by $\frac{L}{\rho U_\infty^2}$, we obtain

$$\left(\frac{\partial u^*}{\partial t^*} + u^*\frac{\partial u^*}{\partial x^*} + v^*\frac{\partial u^*}{\partial y^*}\right) = \frac{\mu}{\rho L U_\infty}\left(\frac{\partial^2 u^*}{\partial x^{*2}} + \frac{\partial^2 u^*}{\partial y^{*2}}\right) \tag{24}$$

Equating equation 39 to 0 , we obtain

$$\left(\frac{\partial u^*}{\partial t^*} + u^*\frac{\partial u^*}{\partial x^*} + v^*\frac{\partial u^*}{\partial y^*}\right) - \frac{\mu}{\rho L U_\infty}\left(\frac{\partial^2 u^*}{\partial x^{*2}} + \frac{\partial^2 u^*}{\partial y^{*2}}\right) = 0 \tag{25}$$

Which is the Non-dimensionlised momentum equation in x direction and $\frac{\mu}{\rho L U_\infty} = \frac{1}{Re}$

G. Discretisation of Momentum Equations in x Direction

Equation 30 is discritised as follows,

$$\int_{t_k}^{t_{k+1}}\int_{y_{(j-\frac{1}{2})}}^{y_{(j+\frac{1}{2})}}\int_{x_{(i-\frac{1}{2})}}^{x_{(i+\frac{1}{2})}}\left\{\frac{\partial u^*}{\partial t^*} + u^*\frac{\partial u^*}{\partial x^*} + v^*\frac{\partial u^*}{\partial y^*} - \frac{\mu}{\rho L U_\infty}\left[\frac{\partial^2 u^*}{\partial x^{*2}} + \frac{\partial^2 u^*}{\partial y^{*2}}\right]\right\}dxdydt \tag{26}$$

Integrating different parts of equation 31 we obtain,

$$\int_{t_k}^{t_{k+1}}\int_{y_{(j-\frac{1}{2})}}^{y_{(j+\frac{1}{2})}}\int_{x_{(i-\frac{1}{2})}}^{x_{(i+\frac{1}{2})}}\frac{\partial u^*}{\partial t^*}dxdydt = \triangle x \triangle y[(u_{k+1}) - (u_k)] \tag{27}$$

Replacement of original 34 has been done below 15.5.21(ignore the statement)

$$\int_{t_{(k)}}^{t_{k+1}}\int_{y_{(j-\frac{1}{2})}}^{y_{(j+\frac{1}{2})}}\int_{x_{(i-\frac{1}{2})}}^{x_{(i+\frac{1}{2})}}u^*\frac{\partial u^*}{\partial x^*}dxdydt = \triangle y \triangle t u_i^*(u_{((i+\frac{1}{2})}^* - u_{(i-\frac{1}{2})}^* = \triangle y \triangle t u_i^*\{(\frac{u_{i+1}^*+u_i^*}{2}) - (\frac{u_i^*+u_{i-1}^*}{2})\} = \frac{\triangle y \triangle t}{2}u_i^*(u_{i+1}^* - u_{i-1}^*) = 0.5Au_i^*(u_{i+1}^* - u_{i-1}^*) \tag{28}$$

$$\int_{t_{(k)}}^{t_{k+1}}\int_{y_{(j-\frac{1}{2})}}^{y_{(j+\frac{1}{2})}}\int_{x_{(i-\frac{1}{2})}}^{x_{(i+\frac{1}{2})}}v^*\frac{\partial u^*}{\partial y^*}dxdydt = \triangle x \triangle t v_j^*(u_{((j+\frac{1}{2})}^* - u_{(j-\frac{1}{2})}^*) = \triangle x \triangle t v_j^*\{(\frac{u_{j+1}^*+u_j^*}{2}) - (\frac{u_j^*+u_{j-1}^*}{2})\} = \frac{\triangle x \triangle t}{2}v_j^*(u_{j+1}^* - u_{j-1}^*) = 0.5Bv_j^*(u_{j+1}^* - u_{j-1}^*) \tag{29}$$

$$\int_{t(k)}^{t(k+1)} \int_{y_{j-\frac{1}{2}}}^{y_{j+\frac{1}{2}}} \int_{x_{i-\frac{1}{2}}}^{x_{i+\frac{1}{2}}} \frac{\partial^2 u^*}{\partial x^{*2}} dx dy dt = \triangle y \triangle t \frac{du^*}{dx^*}\Big|_{(i-\frac{1}{2})}^{(i+\frac{1}{2})} = \triangle y \triangle t (\frac{du^*}{dx^*}\Big|_{(i+\frac{1}{2})} - \frac{du^*}{dx^*}\Big|_{(i-\frac{1}{2})} = \triangle y \triangle t \{(\frac{u_{i+1}^*-u_i^*}{\triangle x}) - (\frac{u_i^*-u_{i-1}^*}{\triangle x} = \triangle y \triangle t(\frac{u_{i+1}^*-2u_i^*+u_{i-1}^*}{\triangle x}) = \frac{\triangle y \triangle t}{\triangle x}(u_{i+1}^* - 2u_i^* + u_{i-1}^*) = Q(u_{i+1}^* - 2u_i^* + u_{i-1}^*) \tag{30}$$

$$\int_{t(k)}^{t(k+1)} \int_{y_{j-\frac{1}{2}}}^{y_{j+\frac{1}{2}}} \int_{x_{i-\frac{1}{2}}}^{x_{i+\frac{1}{2}}} \frac{\partial^2 u^*}{\partial y^{*2}} dx dy dt = \triangle x \triangle t \frac{du^*}{dy^*}\Big|_{(j-\frac{1}{2})}^{(j+\frac{1}{2})} = \triangle x \triangle t (\frac{du^*}{dy^*}\Big|_{(j+\frac{1}{2})} - \frac{du^*}{dy^*}\Big|_{(j-\frac{1}{2})}) = \triangle x \triangle t \{(\frac{u_{j+1}^*-u_j^*}{\triangle y}) - (\frac{u_j^*-u_{j-1}^*}{\triangle y}) = \triangle x \triangle t(\frac{u_{j+1}^*-2u_j^*+u_{j-1}^*}{\triangle y})\} = \frac{\triangle x \triangle t}{\triangle y}(u_{j+1}^* - 2u_j^* + u_{j-1}^*) = R(u_{j+1}^* - 2u_j^* + u_{j-1}^*) \tag{31}$$

Where $A = \triangle y \triangle t, B = \triangle x \triangle t, C = \triangle y \triangle x, Q = \frac{\triangle y \triangle t}{\triangle x}, R = \frac{\triangle x \triangle t}{\triangle y}$.

Combining equations from 28 to 31 , we obtain discretised momentum equation in x direction as

$$C[(u_{(k+1)}) - (u_{(k)})] + 0.5 A u_i^*(u_{(i+1)}^* - u_{(i-1)}^*) + 0.5 B v_j^*(u_{(j+1)}^* - u_{(j-1)}^*) - \frac{\mu}{\rho L U_\infty}\{Q(u_{i+1}^* - 2u_i^* + u_{i-1}^*) + R(u_{j+1}^* - 2u_j^* + u_{j-1}^*)\} = 0 \tag{32}$$

Applying Picards Linearisation method to the non linear equation (34) and simplifying it by dropping * which symbolised non-dmensionlised terms we obtain

$$C[u_{k+1} - u_k] + 0.5 A \bar{u}_i(u_{(i+1)} - u_{(i-1)}) + 0.5 B \bar{v}_j(u_{(j+1)} - u_{(j-1)}) - \frac{\mu_{nf}}{\rho_{nf} L U_\infty}\{Q(u_{i+1} - 2u_i + u_{i-1}) + R(u_{j+1} - 2u_j + u_{j-1})\} = 0 \tag{33}$$

With the presence of nanoparticles and the assumption that they are spherical in shape to guarantee the validity of the Brinkman model and the maxwell model for heat transfer, we compute the effective viscosity of NEPCMs using Brinkman model as follows,

$$\mu_{nf} = \frac{\mu_{PCM}}{(1-\phi)^{2.5}} \tag{34}$$

Where ϕ is the volume fraction of nanoparticles, μ_{PCM} is the dynamic viscosity of pure PCM, and μ_{nf} is the dynamic viscosity of NEPCMs.

H. Non Dimensionlization of Momentum Equations in y Direction
Non dimensionlizing equation 6, momentum equation in y-direction using the given variables

$$x = x^* L \Rightarrow \frac{\partial x^*}{\partial x} = \frac{1}{L}, y = y^* L \Rightarrow \frac{\partial y^*}{\partial y} = \frac{1}{L}, v = v^* U_\infty \Rightarrow \frac{\partial v^*}{\partial x} = 0, T^* = \frac{T-T_\infty}{\triangle T} \Rightarrow T = T^* \triangle T + T_\infty, t^* = \frac{t}{L/U_\infty} \Rightarrow t^* = \frac{t U_\infty}{L} \Rightarrow \frac{\partial t^*}{\partial t} = \frac{U_\infty}{L}, \Rightarrow \frac{\partial v}{\partial t} = U_\infty \frac{\partial v^*}{\partial t^*} \frac{U_\infty}{L}$$

$$\frac{\partial v}{\partial t} = \frac{U_\infty^2}{L} \frac{\partial v^*}{\partial t^*} \tag{35}$$

$$\frac{\partial v}{\partial x} = \frac{\partial(v^* U_\infty)}{\partial x^*} \frac{\partial x^*}{\partial x} = U_\infty \frac{\partial v^*}{\partial x^*} \frac{1}{L} = \frac{U_\infty}{L} \frac{\partial v^*}{\partial x^*} \tag{36}$$

$$\frac{\partial v}{\partial y} = \frac{\partial(v^* U_\infty)}{\partial y^*} \frac{\partial y^*}{\partial y} = U_\infty \frac{\partial v^*}{\partial y^*} \frac{1}{L} = \frac{U_\infty}{L} \frac{\partial v^*}{\partial y^*} \tag{37}$$

$$\frac{\partial^2 v}{\partial x^2} = \frac{\partial}{\partial x}(\frac{\partial v}{\partial x}) = \frac{\partial}{\partial x}(\frac{U_\infty}{L} \frac{\partial v^*}{\partial x^*}) \tag{38}$$

We know $\frac{\partial}{\partial x} = \frac{\partial}{\partial x^*} \frac{\partial x^*}{\partial x}, \frac{\partial x^*}{\partial x} = \frac{1}{L}, \frac{\partial v}{\partial x} = \frac{U_\infty}{L} \frac{\partial v^*}{\partial x^*}$ then we obtain,

$$\frac{\partial^2 v}{\partial x^2} = \frac{\partial}{\partial x}(\frac{\partial v}{\partial x}) = \frac{\partial}{\partial x^*} \frac{\partial x^*}{\partial x}(\frac{U_\infty}{L} \frac{\partial v^*}{\partial x^*} = \frac{U_\infty}{L^2} \frac{\partial^2 v^*}{\partial x^{*2}} \tag{39}$$

We know $\frac{\partial}{\partial y} = \frac{\partial}{\partial y^*} \frac{\partial y^*}{\partial y}, \frac{\partial y^*}{\partial y} = \frac{1}{L}, \frac{\partial v}{\partial y} = \frac{U_\infty}{L} \frac{\partial v^*}{\partial y^*}$ then we obtain,

$$\frac{\partial^2 v}{\partial y^2} = \frac{\partial}{\partial y}(\frac{\partial v}{\partial y}) = \frac{\partial}{\partial y^*} \frac{\partial y^*}{\partial y}(\frac{U_\infty}{L} \frac{\partial v^*}{\partial y^*} = \frac{U_\infty}{L^2} \frac{\partial^2 v^*}{\partial y^{*2}} \tag{40}$$

Substituting equations from (37-42) in equation 3.6 we obtain,

$$\rho(\frac{U_\infty^2}{L} \frac{\partial v^*}{\partial t^*} + u^* U_\infty \frac{U_\infty}{L} \frac{\partial v^*}{\partial x^*} + v^* U_\infty \frac{U_\infty}{L} \frac{\partial v^*}{\partial y^*}) = \mu(\frac{U_\infty}{L^2} \frac{\partial^2 v^*}{\partial x^{*2}} + \frac{U_\infty}{L^2} \frac{\partial^2 v^*}{\partial y^{*2}}) + \beta \rho g(T^* \triangle T + T_\infty - T_r) \tag{41}$$

Simplyfying further, Multiply through by $\frac{L}{\rho U_\infty^2}$

$$\left(\frac{\partial v^*}{\partial t^*} + v^* \frac{\partial v^*}{\partial x^*} + v^* \frac{\partial v^*}{\partial y^*}\right) = \frac{\mu}{\rho L U_\infty}\left(\frac{\partial^2 v^*}{\partial x^{*2}} + \frac{\partial^2 v^*}{\partial y^{*2}}\right) + \frac{L}{U_\infty^2}\beta g(T^* \triangle T + T_\infty - T_r) \tag{42}$$

Rearranging equation 53 , we obtain non dimensionlised momentum equation in y direction

$$\left(\frac{\partial v^*}{\partial t^*} + u^* \frac{\partial v^*}{\partial x^*} + v^* \frac{\partial v^*}{\partial y^*}\right) - \frac{\mu}{\rho L U_\infty}\left(\frac{\partial^2 v^*}{\partial x^{*2}} + \frac{\partial^2 v^*}{\partial y^{*2}}\right) - \frac{L}{U_\infty^2}\beta g(T^* \triangle T + T_\infty - T_r) = 0 \tag{43}$$

I. Discretisation of momentum equations in y direction

Equation (45) is discritised as follows,

$$\int_{t_{(k)}}^{t_{(k+1)}} \int_{y_{(j-\frac{1}{2})}}^{y_{(j+\frac{1}{2})}} \int_{x_{(i-\frac{1}{2})}}^{x_{(i+\frac{1}{2})}} \left\{\frac{\partial v^*}{\partial t^*} + u^* \frac{\partial v^*}{\partial x^*} + v^* \frac{\partial v^*}{\partial y^*} - \frac{\mu}{\rho L U_\infty}\left[\frac{\partial^2 v^*}{\partial x^{*2}} + \frac{\partial^2 v^*}{\partial y^{*2}}\right] - \frac{L}{U_\infty^2}\beta g(T^* \triangle T + T_\infty - T_r)\right\}dxdydt \tag{44}$$

Integrating different parts of equation (46) we obtain,

$$\int_{t_{(k)}}^{t_{(k+1)}} \int_{y_{(j-\frac{1}{2})}}^{y_{(j+\frac{1}{2})}} \int_{x_{(i-\frac{1}{2})}}^{x_{(i+\frac{1}{2})}} \frac{\partial v^*}{\partial t^*} dxdydt = \triangle x \triangle y[(v_{(k+1)}) - (v_{(k)})] \tag{45}$$

$$\int_{t_{(k)}}^{t_{(k+1)}} \int_{y_{(j-\frac{1}{2})}}^{y_{(j+\frac{1}{2})}} \int_{x_{(i-\frac{1}{2})}}^{x_{(i+\frac{1}{2})}} u_i^* \frac{\partial v^*}{\partial x^*} dxdydt = \triangle y \triangle t u_i^*(v_{((i+\frac{1}{2})}^* - v_{(i-\frac{1}{2})}^*) = \triangle y \triangle t u_i^*\{(\frac{v_{i+1}^* + v_i^*}{2}) - (\frac{v_i^* + v_{i-1}^*}{2})\} = \frac{\triangle y \triangle t}{2}u_i^*(v_{(i+1)}^* - v_{(i-1)}^*) = 0.5Au_i^*(v_{(i+1)}^* - v_{(i-1)}^*) \tag{46}$$

Replacement of original (45) is done as follows

$$\int_{t_{(k)}}^{t_{(k+1)}} \int_{y_{(j-\frac{1}{2})}}^{y_{(j+\frac{1}{2})}} \int_{x_{(i-\frac{1}{2})}}^{x_{(i+\frac{1}{2})}} v_j^* \frac{\partial v^*}{\partial y^*} dxdydt = \triangle x \triangle t v_j^*(v_{((j+\frac{1}{2})}^* - v_{(j-\frac{1}{2})}^*) = \triangle x \triangle t v_j^*\{(\frac{v_{j+1}^* + v_j^*}{2}) - (\frac{v_j^* + v_{j-1}^*}{2})\} = \frac{\triangle y \triangle t}{2}v_j^*(v_{(j+1)}^* - v_{(j-1)}^*) = 0.5Bv_j^*(v_{(j+1)}^* - v_{(j-1)}^*) \tag{47}$$

$$\int_{t_{(k)}}^{t_{(k+1)}} \int_{y_{(j-\frac{1}{2})}}^{y_{(j+\frac{1}{2})}} \int_{x_{(i-\frac{1}{2})}}^{x_{(i+\frac{1}{2})}} \frac{\partial^2 v^*}{\partial x^{*2}} dxdydt = \triangle y \triangle t \frac{dv^*}{dx^*}\Big|_{(i-\frac{1}{2})}^{(i+\frac{1}{2})} = \triangle y \triangle t(\frac{dv^*}{dx^*}\Big|_{(i+\frac{1}{2})} - \frac{dv^*}{dx^*}\Big|_{(i-\frac{1}{2})}) = \triangle y \triangle t\{(\frac{v_{i+1}^* - v_i^*}{\triangle x}) - (\frac{v_i^* - v_{i-1}^*}{\triangle x}) = \triangle y \triangle t(\frac{v_{i+1}^* - 2v_i^* + v_{i-1}^*}{\triangle x}) = \frac{\triangle y \triangle t}{\triangle x}(v_{i+1}^* - 2v_i^* + v_{i-1}^*) = Q(v_{i+1}^* - 2v_i^* + v_{i-1}^*) \tag{48}$$

$$\int_{t_{(k)}}^{t_{(k+1)}} \int_{y_{(j-\frac{1}{2})}}^{y_{(j+\frac{1}{2})}} \int_{x_{(i-\frac{1}{2})}}^{x_{(i+\frac{1}{2})}} \frac{\partial^2 v^*}{\partial y^{*2}} dxdydt = \triangle x \triangle t \frac{dv^*}{dy^*}\Big|_{(j-\frac{1}{2})}^{(j+\frac{1}{2})} = \triangle x \triangle t(\frac{dv^*}{dy^*}\Big|_{(j+\frac{1}{2})} - \frac{dv^*}{dy^*}\Big|_{(j-\frac{1}{2})}) = \triangle x \triangle t\{(\frac{v_{j+1}^* - v_j^*}{\triangle y}) - (\frac{v_j^* - v_{j-1}^*}{\triangle y}) = \triangle x \triangle t(\frac{u_{j+1}^* - 2v_j^* + v_{j-1}^*}{\triangle y})\} = \frac{\triangle x \triangle t}{\triangle y}(v_{j+1}^* - 2v_j^* + v_{j-1}^*) = R(v_{j+1}^* - 2v_j^* + v_{j-1}^*) \tag{49}$$

$$\int_{t_{(k)}}^{t_{(k+1)}} \int_{y_{(j-\frac{1}{2})}}^{y_{(j+\frac{1}{2})}} \int_{x_{(i-\frac{1}{2})}}^{x_{(i+\frac{1}{2})}} \frac{L}{U_\infty^2}\beta g(T^* \triangle T + T_\infty - T_r)dxdydt = \triangle x \triangle y \triangle t\{\frac{L}{U_\infty^2}\beta g((T^* \triangle T + T_\infty) - T_r)\} \tag{50}$$

Assembling equations from (45) to (50) together , substituting for $D = \triangle t \triangle x \triangle y$, Applying Picards Linearisation, discarding * we obtain,

$$C[(v_{k+1} - v_k)] + 0.5A\bar{u}_j(v_{i+1} - v_{i-1}) + 0.5B\bar{v}_j(v_{j+1} - v_{j-1}) - \frac{\mu}{\rho_{nf} L U_\infty}\{Q(v_{i+1} - 2v_i + v_{i-1}) + R(v_{j+1} - 2v_j + v_{j-1})\} - D\frac{L}{U_\infty^2}\beta g((T_j \triangle T + T_\infty) - T_r) = 0 \tag{51}$$

J. Non Dimesionlisation and Discretisation of Conservation of Energy Equation

The enthalpy H of PCMs is defined as,

$$H = C_p(T - T_r) + f_l L \tag{52}$$

Where f_l is the PCM liquid fraction and L is the latent heat of the PCMs. By caculating the enthalpy H of PCMs, the liquid fraction and temperature can be updated by the following equations.

$$f_1 = \begin{cases} 0, & H \le H_s \\ \frac{H-H_s}{H_l-H_s}, & H_s \le H < H_l \\ 1, & H \ge H_s \end{cases} \tag{53}$$

$$T = \begin{cases} T = \frac{H_s-H}{c_p}, & H \le H_s \\ T_m, & H_s < H < H \\ T + \frac{H_s-H}{c_p}, & H \le H_s \end{cases} \tag{54}$$

➤ *Non-Dimensionlisation of Conservation of Energy Equation*

$$\frac{\partial(\rho H)}{\partial t^* L/U_\infty}) + \rho c_p[u^* U_\infty \frac{\partial(T^*\Delta T+T_\infty)}{L\partial x^*} + v^* U_\infty \frac{(T^*\Delta T+T_\infty)}{L\partial y^*}] = k[\frac{\partial^2(T^*\Delta T+T_\infty)}{L\partial x^{*2}} + \frac{\partial^2(T^*\Delta T+T_\infty)}{L\partial y^{*2}}] \tag{55}$$

$$\frac{U_\infty}{L}\frac{\partial(\rho H)}{\partial t^*} + \rho c_p[u^* \frac{U_\infty}{L} \frac{\partial(T^*\Delta T+T_\infty)}{\partial x^*} + v^* \frac{U_\infty}{L} \frac{(T^*\Delta T+T_\infty)}{\partial y^*}] = \frac{k}{L}[\frac{\partial^2(T^*\Delta T+T_\infty)}{\partial x^{*2}} + \frac{\partial^2(T^*\Delta T+T_\infty)}{\partial y^{*2}}] \tag{56}$$

Multiply by $\frac{L}{U_\infty}$ ..... $T_\infty = 0$, we obtain,

$$\frac{\partial(\rho H)}{\partial t^*} + \rho c_p[u^* \frac{\partial(T^*\Delta T)}{\partial x^*} + v^* \frac{\partial(T^*\Delta T)}{\partial y^*}] = \frac{k}{U_\infty}[\frac{\partial^2(T^*\Delta T)}{\partial x^{*2}} + \frac{\partial^2(T^*\Delta T)}{\partial y^{*2})}] \tag{57}$$

Multiply by (58) $\frac{1}{\Delta T}$ we obtain,

$$\frac{1}{\Delta T}\frac{\partial(\rho H)}{\partial t^*} + \rho c_p[u^* \frac{\partial T^*}{\partial x^*} + v^* \frac{\partial T^*}{\partial y^*}] = \frac{k}{U_\infty}[\frac{\partial^2 T^*}{\partial x^{*2}} + \frac{\partial^2 T^*}{\partial y^{*2}}] \tag{58}$$

Discretisation of conservation of Energy Equations

$$\int_{t_{(k)}}^{t_{(k+1)}} \int_{y_{(j-\frac{1}{2})}}^{y_{(j+\frac{1}{2})}} \int_{x_{(i-\frac{1}{2})}}^{x_{(i+\frac{1}{2})}} [\frac{1}{\Delta T}\frac{\partial H^*}{\partial t^*} + \rho C_p u^* \frac{\partial T^*}{\partial x^*} + \rho C_p v^* \frac{\partial T^*}{\partial y^*}] dxdydt = \frac{k}{U_\infty} \int_{t_{(k)}}^{t_{(k+1)}} \int_{y_{(j-\frac{1}{2})}}^{y_{(j+\frac{1}{2})}} \int_{x_{(i-\frac{1}{2})}}^{x_{(i+\frac{1}{2})}} [\frac{\partial^2 T^*}{\partial x^{*2}} + \frac{\partial^2 T^*}{\partial y^{*2}}]dxdydt \tag{59}$$

Integrating separate components below we have,

$$\frac{1}{\Delta T}\int_{t_{(k)}}^{t_{(k+1)}} \int_{y_{(j-\frac{1}{2})}}^{y_{(j+\frac{1}{2})}} \int_{x_{(i-\frac{1}{2})}}^{x_{(i+\frac{1}{2})}} \frac{\partial H^*}{\partial t^*} dxdydt = \frac{\Delta x \Delta y}{\Delta T}\{H_{k+1} - H_k\} \tag{60}$$

$$\int_{t_{(k)}}^{t_{(k+1)}} \int_{y_{(j-\frac{1}{2})}}^{y_{(j+\frac{1}{2})}} \int_{x_{(i-\frac{1}{2})}}^{x_{(i+\frac{1}{2})}} u_i^* \frac{\partial T^*}{\partial x^*} dxdydt = \Delta y \Delta t u_i^*(T_{((i+\frac{1}{2})}^* - T_{(i-\frac{1}{2})}^*) = \Delta y \Delta t u_i^*\{(\frac{T_{i+1}^*-T_i^*}{2}) - (\frac{T_i^*-T_{i-1}^*}{2})\} = \frac{\Delta y \Delta t}{2}u_i^*(T_{(i+1)}^* - T_{(i-1)}^*) \tag{61}$$

$$\int_{t_{(k)}}^{t_{(k+1)}} \int_{y_{(j-\frac{1}{2})}}^{y_{(j+\frac{1}{2})}} \int_{x_{(i-\frac{1}{2})}}^{x_{(i+\frac{1}{2})}} v_j^* \frac{\partial T^*}{\partial y^*} dxdydt = \Delta x \Delta t v_j^*(T_{((j+\frac{1}{2})}^* - T_{(j-\frac{1}{2})}^*) = \Delta x \Delta t v_j^*\{(\frac{T_{j+1}^*-T_j^*}{2}) - (\frac{T_j^*-T_{j-1}^*}{2})\} = \frac{\Delta x \Delta t}{2}v_j^*(T_{(j+1)}^* - T_{(j-1)}^*) \tag{62}$$

$$\int_{t_{(k)}}^{t_{(k+1)}} \int_{y_{(j-\frac{1}{2})}}^{y_{(j+\frac{1}{2})}} \int_{x_{(i-\frac{1}{2})}}^{x_{(i+\frac{1}{2})}} \frac{\partial^2 T^*}{\partial x^{*2}} dxdydt = \Delta y \Delta t \frac{dT^*}{dx^*}|_{i-\frac{1}{2}}^{i+\frac{1}{2}} = \Delta y \Delta t (\frac{dT^*}{dx^*}|_{i+\frac{1}{2}} - \frac{dT^*}{dx^*}|_{i-\frac{1}{2}}) = \Delta y \Delta t\{(\frac{T_{i+1}^*-T_i^*}{\Delta x}) - (\frac{T_i^*-T_{i-1}^*}{\Delta x})\} = \Delta y \Delta t(\frac{T_{i+1}^*-2T_i^*+T_{i-1}^*}{\Delta x} \tag{63}$$

$$\int_{t_{(k)}}^{t_{(k+1)}} \int_{y_{(j-\frac{1}{2})}}^{y_{(j+\frac{1}{2})}} \int_{x_{(i-\frac{1}{2})}}^{x_{(i+\frac{1}{2})}} \frac{\partial^2 T^*}{\partial y^{*2}} dxdydt = \Delta x \Delta t \frac{dT^*}{dy^*}|_{j-\frac{1}{2}}^{j+\frac{1}{2}} = \Delta x \Delta t (\frac{dT^*}{dy^*}|_{j+\frac{1}{2}} - \frac{dT^*}{dx^*}|_{j-\frac{1}{2}}) = \Delta x \Delta t\{(\frac{T_{j+1}^*-T_j^*}{\Delta y}) - (\frac{T_j^*-T_{j-1}^*}{\Delta y})\} = \Delta x \Delta t(\frac{T_{j+1}^*-2T_j^*+T_{j-1}^*}{\Delta y} \tag{64}$$

Hence discretised energy equation is

$$\frac{\Delta x \Delta y}{\Delta T}\{H_{k+1} - H_k\} + 0.5A\rho(C_p)u_i^*(T_{(i+1)}^* - T_{(i-1)}^*) + 0.5B\rho(C_p)v_j^*(v_{(j+1)}^* - T_{(j-1)}^*) = \frac{k}{U_\infty}\{Q(T_{i+1}^* - 2T_i^* + T_{i-1}^*) + R(T_{j+1}^* - 2T_j^* + T_{j-1}^*)\}$$

(65)

Where $S = \frac{\Delta x \Delta y}{\Delta T}$, the simplified discretised energy equation is,

$$S(H_{k+1} - H_k) + 0.5A\rho(C_p)u_i(T_{(i+1)} - T_{(i-1)}) + 0.5B\rho(C_p)v_j(T_{(j+1)} - T_{(j-1)}) = \frac{k}{U_\infty}\{Q(T_{i+1} - 2T_i + T_{i-1}) + R(T_{j+1} - 2T_j + T_{j-1})\}$$

(66)

The thermal conductivity of NEPCM is calculated according to the Maxwell model as

$$k_{nf} = k_{PCM}\frac{k_p + 2k_{PCM} - 2(k_{PCM} - k_p)\phi}{k_p + 2k_{PCM} + (k_{PCM} - k_p)\phi}$$

(67)

Where k_{PCM}, k_p, and k_{nf} are thermal conductivities of pure PCMs, nanoparticles and NEPCMs respectively. The density of nano-fluid ρ_{nf} is calculated as

$$\rho_{nf} = (1 - \phi)\rho_{PCM} + \phi\rho_p$$

(68)

Where ρ_{PCM}, and ρ_p are densities of pure and nanoparticles. The heat capacitance of NEPCMs $(\rho c_p)_{nf}$ is defined as

$$(\rho c_p)_{nf} = (1 - \phi)(\rho c_p)_{PCM} + \phi(\rho c_p)_p$$

(69)

Where $(\rho c_p)_{PCM}$ is the heat capacitance of the PCM, and $(\rho c_p)_p$ is the heat capacitance of nanoparticles. thermal expansion volume of NEPCMs $(\rho\beta)_{nf}$ is given as

$$(\rho\beta)_{nf} = (1 - \phi)(\rho\beta)_{PCM} + \phi(\rho\beta)_p$$

(70)

Where $(\rho\beta)_{PCM}$ and $(\rho\beta)_p$ are thermal expansion volume of pure PCM and nanoparticles respectively. The latent heat of NEPCMs is computed as

$$(\rho L)_{nf} = (1 - \phi)(\rho L)_{PCM}$$

(71)

Where $(\rho L)_{PCM}$ is the latent heat of pure PCM. Then the corresponding enthalpy of NEPCM H_{nf} is given as

$$H_{nf} = Cp_{nf}(T - T_r) + f_l L_{nf}$$

(72)

IV. RESULTS

A. Parameter Estimation
The numerical simulations depends on the following parameters estimated in Table I.

Table 1: Parameter Estimation (Estimation is based on Sodium Chloride)

| Parameter	Description	Value range	Value used	Source
ρ_p	Density of nanoparticles (sodium chloride)	2.16 g/cm3	2.16 g/cm3	[19]
ρ_{PCM}	Density of pure PCM	2.26 g/cm3	2.26 g/cm3	[29, 10]
Cp	Heat capacity	0.849-0.9 (J/Kg K)	0.86	[24, 13]
β_{PCM}	Coefficient of Thermal expansion volume of pure PCM	-	0.064 (W/m -K)	[4]
β_p	Coefficient of Thermal expansion volume of nanoparticles	$3.96 - 5.63 \times 10^{-5}K^{-1}$	$4.5 \times 10^{-5}K^{-1}$	[26]
k	Thermal conductivity	3.13-3.87 W/m K	3.5 W/m K	[24, 9]

B. Numerical Simulations
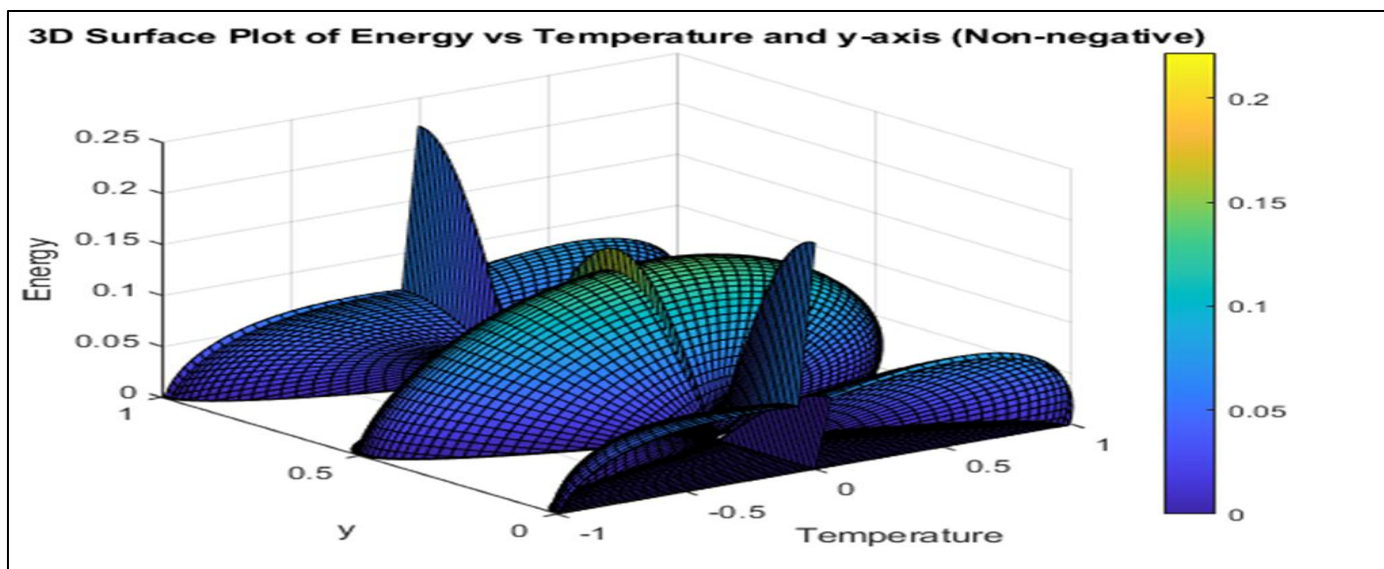
Fig. 1: Surface Plot of Energy vs Temperature and y-Axis

Fig. 4 presents a 3D surface plot illustrating the relationship between 'Energy' and 'Temperature' at various points along the 'y' axis within a thermal energy storage system, potentially involving phase change materials (PCMs). The plot demonstrates how nano-particles impact energy storage characteristics. The z-axis represents thermal energy, indicating energy absorbed or released during phase changes like melting. The y-axis denotes material positions or layers with varying nano-particle concentrations. The x-axis indicates PCM temperature crucial for phase transitions. Peaks signify significant energy storage changes, likely corresponding to phase change temperatures. Color gradient (blue to yellow) reflects energy magnitude, aiding in identifying efficient energy storage regions. The analysis targets PCM optimization for applications like solar energy and heating systems.
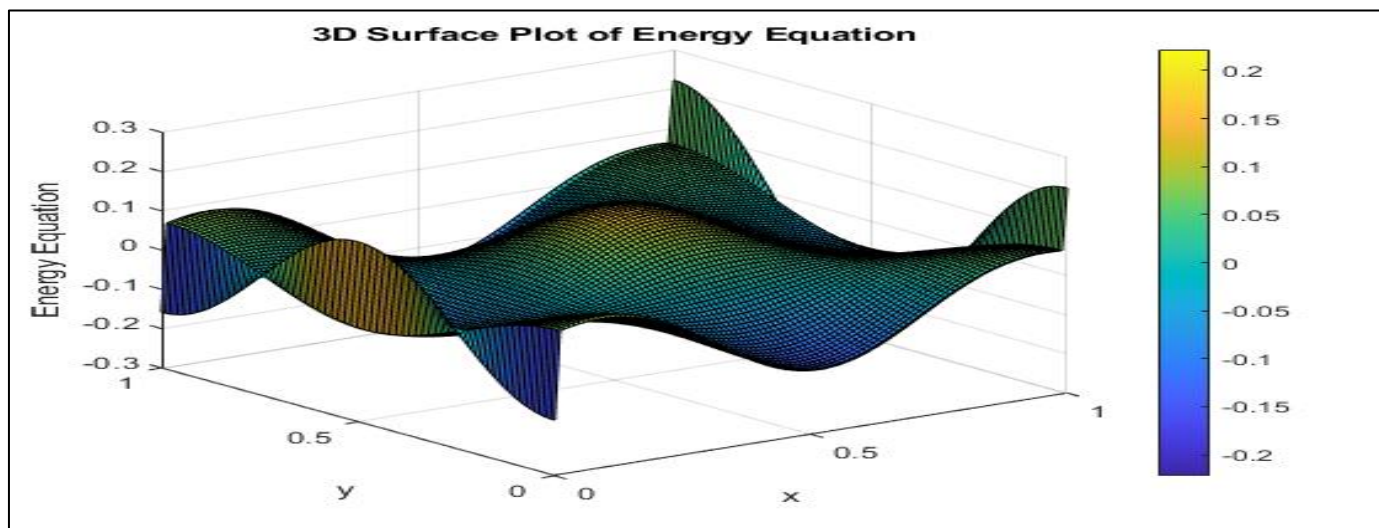

Fig. 5: 3D Surface Plot of Energy Equation

Fig. 5 shows a 3D surface plot representing a function describing energy variation across 'x' and 'y' axes, indicating spatial dimensions or relevant parameters within a nano-enhanced Phase Change Material (PCM) for thermal energy storage. The z-axis depicts energy Evaluation, showing energy changes within the material, crucial for PCMs storing and releasing energy during phase transitions like melting. The plot indicates regions where energy storage behavior alters due to nano-particle incorporation. Peaks signify areas of intense energy interaction, indicating efficient heat transfer or latent heat release/absorption. The color bar reflects energy change magnitude, from blue (negative values) to yellow (positive values), suggesting both energy absorption and release. These analyses could aid in optimizing PCM design for applications like passive climate control or thermal regulation in electronics, ensuring efficient heat absorption and release for stable environments or component protection.
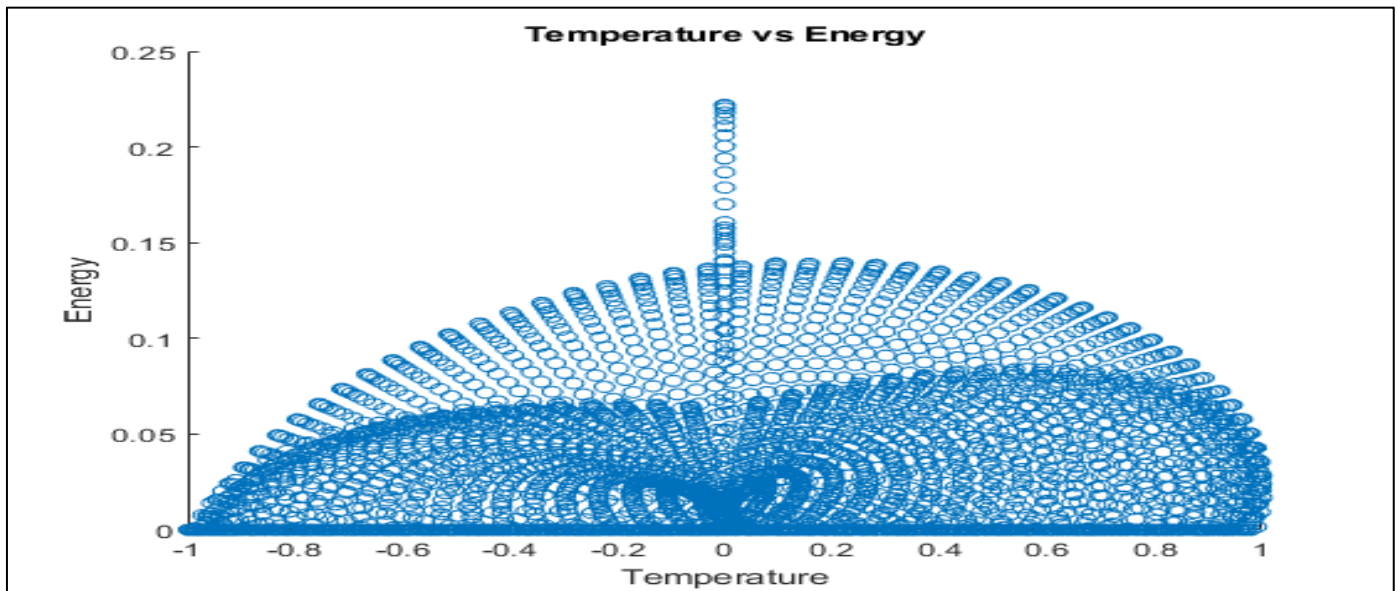
Fig. 6: Energy Against Temperature

Fig. 6 shows a scatter plot illustrating the relationship between temperature and energy for nano-enhanced PCMs in thermal energy storage. The data forms curves representing varied experimental conditions and nanoparticle concentrations. The semicircular arrangement suggests cyclic energy changes with temperature, typical of PCM melting and solidification cycles. Each semicircle reflects a phase change cycle, indicating energy absorption or release. Clustering at specific temperatures suggests phase transition points, which are typical of PCM behavior. The plot emphasizes energy absorption, as all values are positive, likely depicting only one side of the phase change process. This analysis could be vital for optimizing nano-enhancements aiming to improve PCM thermal conductivity and reduce supercooling, enhancing thermal storage capacity and heat transfer efficiency. Such insights aid in optimizing PCM design for applications in heating, cooling, waste heat recovery, and electronics thermal management.

V. CONCLUSION

The analysis of nano-enhanced PCMs for thermal energy storage involves understanding the relationship between temperature, energy, and the spatial distribution of nanoparticles within the PCM. Fig. 4 and Fig. 5 present 3D surface plots that illustrate these relationships. They show how energy storage characteristics are influenced by temperature and spatial variables, with peaks in the plots likely indicating phase change temperatures where significant energy absorption or release occurs. The scatter plot in Figure 5 provides a visual representation of the cyclic energy changes associated with the phase transitions of PCMs. The semicircular patterns could reflect the material's energy absorption during the phase change, with clustering at specific temperatures indicative of phase transition points. Figure 6 portrays a symmetric curve of energy against a spatial variable 'y', suggesting a uniform distribution of the nano-enhancement effects across the PCM. The central peak represents the point of maximum energy interaction, and the

variation from negative to positive values indicates the energy absorption and release phases. These visual data representations are crucial for the optimization of PCM performance in thermal energy storage systems. They guide improvements in thermal conductivity and heat capacity, essential for applications such as solar energy systems, heating and cooling, waste heat recovery, and thermal management in electronics. Enhanced PCMs have the potential to maintain stable temperatures in various applications, contributing to energy efficiency and sustainability.

Enthalpy and temperature are directly correlated in nano-enhanced PCMs, with the phase change process significantly impacting the enthalpy due to heat absorption or release. Although velocity is not directly referenced, the enhanced heat transfer due to nanoparticles indirectly affects the rate of heat transfer, promoting temperature uniformity. Future recommendations for nano-enhanced PCMs in thermal energy storage should employ advanced numerical methods and simulation tools to predict the performance of nano-enhanced PCMs more accurately. This would aid in understanding the complex interactions within the PCM and in optimizing the material properties before experimental validation

REFERENCES

[1].   N Ahmed, KE Elfeky, Lin Lu, and QW Wang. Thermal performance analysis of thermocline combined sensible-latent heat storage system using cascaded-layered pcm designs for medium temperature applications. *Renewable Energy*, 152:684–697, 2020.

[2].   BR Baliga and SV Patankar. A new finite-element formulation for convection-diffusion problems. *Numerical Heat Transfer*, 3(4):393–409, 1980.

[3].   Yuri Bazilevs and Thomas JR Hughes. Weak imposition of dirichlet boundary conditions in fluid mechanics. *Computers & fluids*, 36(1):12–26, 2007.

[4]. J Chiew, CS Chin, WD Toh, Z Gao, and J Jia. Thermal state-of-expansion or melting of phase change material based heat sink for underwater battery power system. *Journal of Energy Storage*, 26:100956, 2019.

[5]. Sandra Raquel Leite da Cunha and José Lu1ǯ3053′fs Barroso de Aguiar. Phase change materials and energy efficiency of buildings: A review of knowledge. *Journal of Energy Storage*, 27:101083, 2020.

[6]. Karem Elsayed Elfeky, Abubakar Gambo Mohammed, and Qiuwang Wang. Cycle cut-off criterion effect on the performance of cascaded, sensible, combined sensible-latent heat storage tank for concentrating solar power plants. *Energy*, 230:120771, 2021.

[7]. Moritz Gosses, Wolfgang Nowak, and Thomas Wöhling. Explicit treatment for dirichlet, neumann and cauchy boundary conditions in pod-based reduction of groundwater models. *Advances in water resources*, 115:160–171, 2018.

[8]. Marcus J Grote and Christoph Kirsch. Dirichlet-to-neumann boundary conditions for multiple scattering problems. *Journal of Computational Physics*, 201(2):630–650, 2004.

[9]. Zhidong Han and Alberto Fina. Thermal conductivity of carbon nanotubes and their polymer nanocomposites: A review. *Progress in polymer science*, 36(7):914–944, 2011.

[10]. Feng Hou, Xinjuan Zhao, Hui Wang, and Qinxi Dong. Microstructure-guided computational model for predicting effective thermal conductivity of cementitious composites filled with phase change particles. *Case Studies in Thermal Engineering*, 38:102339, 2022.

[11]. Amin Ramiani Jafari. Phase change modelling with flexible source-based kinetics for non-equilibrium transitions. *International Journal of Thermal Sciences*, 159:106608, 2021.

[12]. Hussam Jouhara, Alina Żabnieńska-Góra, Navid Khordehgah, Darem Ahmad, and Tom Lipinski. Latent thermal energy storage technologies and applications: A review. *International Journal of Thermofluids*, 5:100039, 2020.

[13]. Cao JX, Yan XH, and Y Xiao. Specific heat of single-walled carbon nanotubes: A lattice dynamics study. *Journal of the Physical Society of Japan*, 72(9):2256–2259, 2003.

[14]. JWJ Kaiser, S Adami, IS Akhatov, and NA Adams. A semi-implicit conservative sharp-interface method for liquid-solid phase transition. *International Journal of Heat and Mass Transfer*, 155:119800, 2020.

[15]. Karunesh Kant, Amritanshu Shukla, Atul Sharma, and Pascal Henry Biwole. Heat transfer studies of photovoltaic panel coupled with phase change material. *Solar Energy*, 140:151–161, 2016.

[16]. Sameer Khare, Mark Dell'Amico, Chris Knight, and Scott McGarry. Selection of materials for high temperature latent heat energy storage. *Solar energy materials and solar cells*, 107:20–27, 2012.

[17]. Rahul Khatri, Rahul Goyal, and Ravi Kumar Sharma. Advances in the developments of solar cooker for sustainable development: A comprehensive review. *Renewable and Sustainable Energy Reviews*, 145:111166, 2021.

[18]. Dai Liu, Long Xin-Feng, Lou Bo, Zhou Si-quan, and Xu Yan. Progress in thermochemical energy storage for concentrated solar power: A review. *International journal of energy research*, 42(15):4546–4561, 2018.

[19]. Maoyuan Liu, Patrick Masset, and Angus Gray-Weale. Solubility of sodium in sodium chloride: a density functional theory molecular dynamics study. *Journal of The Electrochemical Society*, 161(8):E3042, 2014.

[20]. D Lopes, R Agujetas, Hélder Puga, J Teixeira, R Lima, JP Alejo, and C Ferrera. Analysis of finite element and finite volume methods for fluid-structure interaction simulation of blood flow in a real stenosed artery. *International Journal of Mechanical Sciences*, 207:106650, 2021.

[21]. Sidi El Becaye Maiga, Samy Joseph Palm, Cong Tam Nguyen, Gilles Roy, and Nicolas Galanis. Heat transfer enhancement by using nanofluids in forced convection flows. *International journal of heat and fluid flow*, 26(4):530–546, 2005.

[22]. Dnyaneshwar Malwad and Vinod Tungikar. Experimental performance analysis of an improved receiver for scheffler solar concentrator. *SN Applied Sciences*, 2:1–14, 2020.

[23]. Nele Moelans, Bart Blanpain, and Patrick Wollants. An introduction to phase-field modeling of microstructure evolution. *Calphad*, 32(2):268–294, 2008.

[24]. Paul E Ohlsen. Thermal conductivity of sodium chloride within the temperature range 375 k to 637 k. 1956.

[25]. Christos Pagkalos, George Dogkas, Maria K Koukou, John Konstantaras, Kostas Lymperis, and Michail Gr Vrachopoulos. Evaluation of water and paraffin pcm as storage media for use in thermal energy storage applications: A numerical approach. *International Journal of Thermofluids*, 1:100006, 2020.

[26]. SS Parker, NM Abdul-Jabbar, JM Jackson, and M Monreal. Feasibility of volumetric expansion of molten chlorides by conventional pushrod dilatometry. *Journal of Radioanalytical and Nuclear Chemistry*, 331(12):5259–5263, 2022.

[27]. R. Jay Patel, Manish K Rathod, Rajvikram Madurai Elavarasan, and Zafar Said. Influence of longitudinal fin arrangement on the melting and solidification inside the triplex tube latent heat thermal storage system. *Journal of Energy Storage*, 46:103778, 2022.

[28]. Manish K Rathod and Jyotirmay Banerjee. Thermal stability of phase change materials used in latent heat energy storage systems: A review. *Renewable and sustainable energy reviews*, 18:246–258, 2013.

[29]. Zafar Said, Hanin Zeyad, Tasnim I Eisa, and Mamdouh EL Haj Assad. Nano-enhanced pcm for energy storage. In *2019 Advances in Science and Engineering Technology International Conferences (ASET)*, pages 1–6. IEEE, 2019.

[30]. Atul Sharma, V Veer Tyagi, Carl R Chen, and Dharam Buddhi. Review on thermal energy storage with phase change materials and applications. *Renewable and Sustainable energy reviews*, 13(2):318–345, 2009.

[31]. Paul S Sheeran, Juan D Rojas, Connor Puett, Jordan Hjelmquist, Christopher B Arena, and Paul A Dayton. Contrast-enhanced ultrasound imaging and in vivo circulatory kinetics with low-boiling-point nanoscale phase-change perfluorocarbon agents. *Ultrasound in medicine & biology*, 41(3):814–831, 2015.

[32]. Farooq Sher, Oliver Curnick, and Mohammad Tazli Azizan. Sustainable conversion of renewable energy sources, 2021.

[33]. Asfafaw H Tesfay, Mulu B Kahsay, and Ole J Nydal. Solar cookers with latent heat storage for intensive cooking application. In *ISES Proceedings of Solar World Congress, Daegu, Korea*, volume 8, pages 71–79, 2015.

[34]. Michael Vollmer. Physics of the electromagnetic spectrum. *Electromagnetic technologies in food science*, pages 1–32, 2021.

[35]. Mazlan Abdul Wahid, Seyed Ehsan Hosseini, Hasanen M Hussen, Hussein J Akeiber, Safaa N Saud, and Abdulrahman Th Mohammad. An overview of phase change materials for construction architecture thermal management in hot and dry climate region. *Applied thermal engineering*, 112:1240–1259, 2017.

[36]. Fuzhang Wang, RS Varun Kumar, G Sowmya, Essam Roshdy El-Zahar, BC Prasannakumara, M Ijaz Khan, Sami Ullah Khan, MY Malik, and Wei-Feng Xia. Lsm and dtm-pade approximation for the combined impacts of convective and radiative heat transfer on an inclined porous longitudinal fin. *Case Studies in Thermal Engineering*, 35:101846, 2022.

[37]. Xin Wang, Min Luo, Harshinie Karunarathna, and Dominic E Reeve. An enhanced momentum conservation treatment for fdm simulation of two-phase flows with large density ratio. *Journal of Computational Physics*, 478:111949, 2023.

[38]. M Grae Worster. Instabilities of the liquid and mushy regions during solidification of alloys. *Journal of Fluid Mechanics*, 237:649–669, 1992.

[39]. Shaofei Wu, Ting Yan, Zihan Kuai, and Weiguo Pan. Thermal conductivity enhancement on phase change materials for thermal energy storage: A review. *Energy Storage Materials*, 25:251–295, 2020.

[40]. Lu-Yao Yang, Chang-Ping Feng, Lu Bai, Rui-Ying Bao, Zheng-Ying Liu, Ming-Bo Yang, and Wei Yang. Flexible shape-stabilized phase change materials with passive radiative cooling capability for thermal management. *Chemical Engineering Journal*, 425:131466, 2021.

[41]. Sheng Yang, Xue-Feng Shao, Jia-Hao Luo, Seyedmohsen Baghaei Oskouei, Özgür Bayer, and Li-Wu Fan. A novel cascade latent heat thermal energy storage system consisting of erythritol and paraffin wax for deep recovery of medium-temperature industrial waste heat.

[42]. Zohir Younsi and Hassane Naji. A numerical investigation of melting phase change process via the enthalpy-porosity approach: Application to hydrated salts. *International Communications in Heat and Mass Transfer*, 86:12–24, 2017.

[43]. Malik Sarmad Zahid, Naveed Ahmed, Mumtaz A Qaisrani, Mariam Mahmood, Majid Ali, Adeel Waqas, and Mohsen Assadi. Charging and discharging characterization of a novel combined sensible-latent heat thermal energy storage system by experimental investigations for medium temperature applications. *Journal of Energy Storage*, 55:105612, 2022.

[44]. Mostafa M Zaytoun, Mohaned M El-Bashouty, Medhat M Sorour, and Mohamed A Alnakeeb. Heat transfer characteristics of pcm inside a modified design of shell and tube latent heat thermal energy storage unit. *Case Studies in Thermal Engineering*, 49:103372, 2023.

[45]. Myrto Zeneli, Aris Nikolopoulos, Sotirios Karellas, and Nikolaos Nikolopoulos. Numerical methods for solid-liquid phase-change problems. In *Ultra-high temperature thermal energy storage, transfer and conversion*, pages 165–199. Elsevier, 2021.

[46]. Shuai Zhang, Daili Feng, Lei Shi, Li Wang, Yingai Jin, Limei Tian, Ziyuan Li, Guoyong Wang, Lei Zhao, and Yuying Yan. A review of phase change heat transfer in shape-stabilized phase change materials (ss-pcms) based on porous supports for thermal energy storage. *Renewable and Sustainable Energy Reviews*, 135:110127, 2021.

[47]. Pengbo Zhao, Renkun Dai, Wei Li, Qiuwang Wang, and Min Zeng. Modeling the mushy zone during the melting process under neumann boundary condition using the improved enthalpy-porosity method. *Numerical Heat Transfer, Part A: Applications*, 78(8):423–442, 2020.